# Chapter 1

# Solar Coronagraphs

Douglas Rabin
*NASA Goddard Space Flight Center, Heliophysics Science Division,*
*Greenbelt, Maryland 20771, USA*
*douglas.rabin@nasa.gov*

A solar coronagraph enables study of the Sun's tenuous outer atmosphere—the corona—by occulting the brilliant solar disk. We describe scientific objectives of solar coronagraphy; measurement requirements that follow from those objectives; instrument design principles to effectuate the required measurements; and some aspects of the practical implementation of these principles in space- and ground-based instruments.

## 1. Scientific Objectives

The gross internal structure of a star like the Sun is relatively well understood and confirmed by helioseismic measurements.[1] The largest gap in our understanding is the time-dependent interaction of convection with magnetic fields, which in the Sun gives rise to a quasi-periodic dynamo, magnetic concentrations such as sunspots, active regions, and network fields, and a large-scale magnetic field extending above the visible-light surface (the photosphere) into the heliosphere. Equilibrium thermodynamics suggests that the temperature of the solar plasma should decrease monotonically from the core ($\sim$15 MK) outward, as indeed it does—until just above the photosphere, where the average temperature increases outward in less than $10^4$ km from a minimum of about 4300 K to over 1 MK in the corona. It is widely agreed that the magnetic field plays an essential role in creating the corona, but the mechanisms by which this is achieved remain the subject of research.[2]

The observed corona is highly structured and dynamic, again because of the Sun's magnetic field.[3] Characteristic structures seen repeatedly in coronal images have acquired descriptive names, such as "loop", "streamer", "plume" or "jet."[4] It is difficult to measure the coronal magnetic field directly.[5,6] However, the gas and the magnetic field are tied together because of the high electrical conductivity of coronal plasma, and luminous coronal features indicate the direction of the field projected onto the plane of the sky. Figure 1 shows the inner corona as seen in broadband visible light during a total eclipse;[7] the plasma is made visible by Thomson scattering of photospheric light off free electrons.[8] Figure 2 is a different

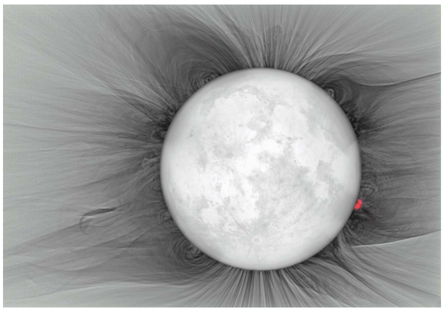

Fig. 1. Negative composite image of the white-light corona during the total solar eclipse of 11 July 2010.[7] The coronal image has been enhanced with specially tailored unsharp masking; the lunar image is superimposed.

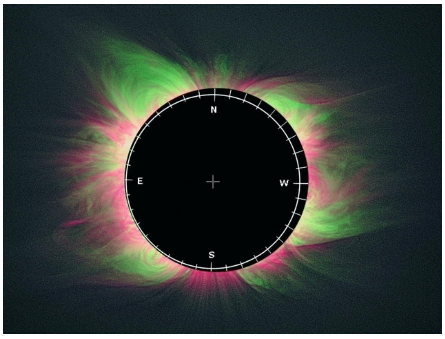


Fig. 2. Composite false-color image from the eclipse of 11 July 2010.[7] Redder regions are hotter (dominated by Fe XIV emission at 530.3 nm) than green regions (dominated by Fe X emission at 637.4 nm).

view during the same eclipse afforded by visible-light forbidden emission lines of iron that differentiate regions by temperature.[7] The inner corona (out to 1.5–2.5 $R_\odot$) is often visualized in the light of one or more ultraviolet or extreme ultraviolet (EUV) allowed emission lines, as in Fig. 3; an occulter is not needed because the radiance from the solar disk is not much different from the radiance above the limb. EUV emission is typically too faint to be detected at larger radii, where a “white light” (Thomson scattering) coronagraph is still effective (Fig. 4).

Coronagraphy is an important tool for investigating all the major scientific questions concerning the solar corona, including:

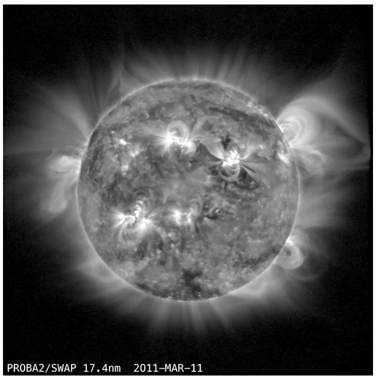


Fig. 3. EUV image of the corona obtained by the SWAP camera on the PROBA-2 spacecraft.[9] The narrow bandpass is dominated by emission from Fe IX–XI.

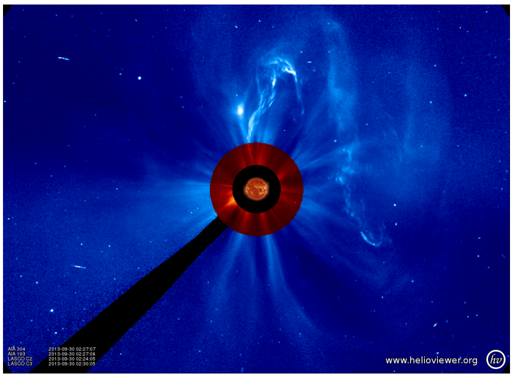


Fig. 4. Composite image of a coronal mass ejection.[10] Solar disk: AIA EUV imager on the SDO spacecraft. Red annular image: LASCO C2 coronagraph on the SOHO spacecraft. Blue image: LASCO C3 coronagraph. The boom holding the external C3 occulter is visible on the left.

- How is the gas heated? How does it cool?
- How does mass enter? How does it leave? From what kinds of regions does the solar wind[11] emanate?
- What causes solar flares[12] and coronal mass ejections?[13]
- How are different types of coronal structures created and destroyed, and what are the spatial and temporal scales most important to their evolution? How do structures composed primarily of neutral matter persist in the million-degree corona, sometimes for weeks?
- How does magnetic reconnection[14] operate in the corona? How does turbulence operate?
- How do mass ejections evolve as they propagate outward, creating "space weather"[15] in the heliosphere and at Earth?

## 2. Scope

For the purposes of this review, a coronagraph is an imager that is required to block (occult) light from the solar photosphere because the photosphere is much brighter than the corona in the imaging bandpass. White light coronagraphs[a] will be emphasized because they are the most widely used and exemplify the key design challenges and approaches. Heliospheric imagers are specialized wide-angle coronagraphs designed to image the heliosphere from $\gtrsim 10\ R_\odot$ to the Earth ($215\ R_\odot$);[16] they have much in common with conventional coronagraphs but pose particular design challenges not addressed here. We cite specific coronagraphs to illustrate design principles but do not attempt a census of existing instruments.

A non-solar coronagraph can resemble a solar coronagraph but may also be quite different.[b] The bright source to be occulted by a "stellar" coronagraph may often be treated as a point source, and the object or objects to be studied—*e.g.*, exoplanets—may be at known locations or in preferred radial or angular zones, facts that can be exploited by tailored apodization of the coronagraph entrance pupil. By contrast, a solar coronagraph must occult an extended source, and the objects of study are typically widely distributed in radius and position angle with respect to the center of the Sun.

Stray light in an imaging system is, broadly, light that reaches the focal plane by other than idealized ray paths such as those of geometrical optics. Under that definition, diffraction, unwanted specular reflection, and scattering (transmissive or reflective) are sources of stray light. Diffraction is always important in a coronagraph and will be considered below. Non-diffractive stray light is usually just as important but is less amenable to systematic treatment because the means to suppress it are highly dependent on the particulars of the coronagraph and its environment. Reference 17 is a general treatment of stray light analysis and control.

[a] "White light" refers to the wavelength-independent cross section for Thomson scattering. The coronagraph bandpass may be wide or narrow.
[b] See Volume 3, Chapters 18-20.

The focal-plane sensor, post-sensor electronics, and data processing are essential components of a coronagraph system. We consider the sensor with respect to signal and noise, but little else about the post-focus chain can be generalized.

We are not aware of a recent general review of solar coronagraphs. An older survey may be found in the monograph by Billings.[8] Reference 18 is a lucid explication of optical design principles for an externally and internally occulted coronagraph.

## 3. Measurement Requirements

### 3.1. *Signal and Backgrounds*

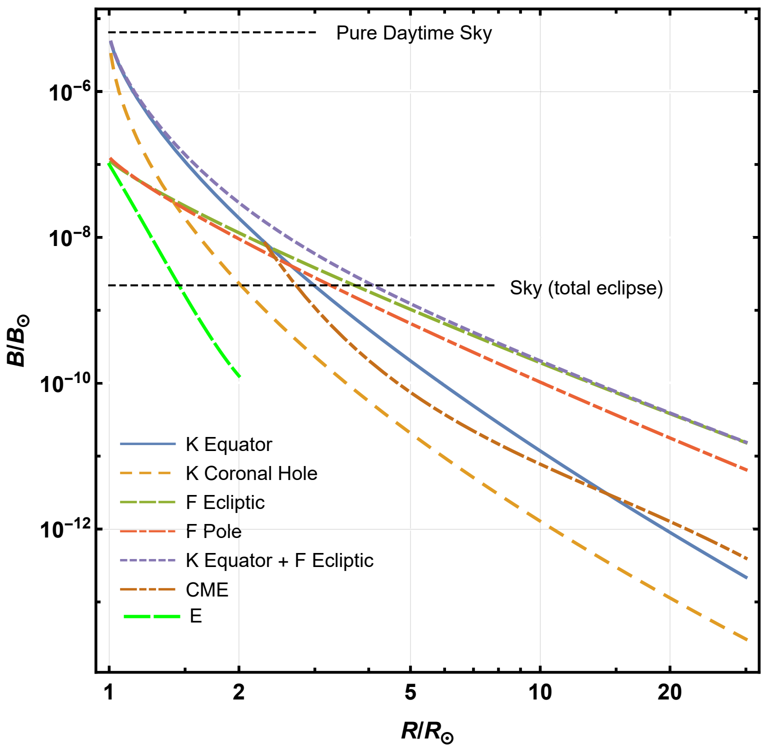


Fig. 5. Radiance of various components of the solar corona in units of the mean radiance of the solar disk ($B_\odot$) in the bandpass 400–600 nm.[19] Also shown are the typical radiance of the sky near the Sun at a very high-quality ground-based observing site outside eclipse and during total eclipse.[19,20]

Traditional nomenclature distinguishes between the K- (Kontinuierlich) corona, the F- (Fraunhofer) corona, and the E- (Emission) corona.[21] The K- and E- components arise from coronal plasma and correspond to the electron scattering and atomic emission mechanisms discussed above. The F-corona, also known as zodiacal light, corresponds to scattering of photospheric light off interplanetary dust concentrated near the ecliptic plane.[22] For a solar coronagraph, the F-corona is background rather than signal.

Because the K-corona has the same spectral distribution as the photosphere[c], its signal can be expressed relative to the mean radiance of the solar disk ($B_\odot$) without specifying the band pass. This is approximately true of the F-corona in the visible region of the spectrum although not in the thermal infrared, where zodiacal dust is a source of emission. Figure 5 shows radiances in the bandpass 400–600 nm for the K-corona (at the solar equator or in a coronal hole) and the F-corona (in the ecliptic plane or at the ecliptic pole).[23] Because the complex structures evident in Figs. 1–4 change over hours and days as well as systematically through the course of a solar activity cycle, the curves in Fig. 5 should be regarded more as approximate boundaries than as radiances typical of a particular solar latitude. Also shown in Fig. 5 is a curve representing the typical radiance of a coronal mass ejection.[16] The radiance of CMEs varies widely; the curve mainly serves to emphasize that, for transient features, the signal to be measured is often only a small fraction of the local quasi-steady K-coronal radiance, which is in turn dominated by background light for $R \gtrsim 2.5\ R_\odot$.

In the visible region, the E-corona is observed through narrow filters, each centered on a wavelength dominated by a single emission line (Fig. 2); otherwise the signal is overwhelmed by the broad-band K+F corona. In the EUV, the continuum background is much weaker, but a bandpass filter (typically a multilayer coating on a mirror) is still necessary to restrict the signal to a few dominant emission lines (Fig. 3); otherwise it is difficult to relate the signal to the temperature structure of the gas.

## 3.2. *Polarization*

### 3.2.1. *Sources of Polarization*

Linear polarization is an important physical diagnostic and instrument design tool throughout the corona. Both circular and linear polarization can be used to infer the strength and direction of the magnetic field in the inner corona ($R \lesssim 2\ R_\odot$), but the measurements are challenging and require a large-aperture ($\gtrsim 1$ m) telescope.[24–26] Although direct photospheric light averaged over the solar disk is essentially unpolarized, the K-corona exhibits a high degree of linear polarization. As summarized by Ref. 8,

> If the Sun were a point source of light and the corona a small aggregate of scattering material lying at the vertex of a right angle between the Sun and the observer, the scattered radiation would be 100% polarized, with its electric vector normal to the plane containing the incident and the scattered rays.

Because the Sun is an extended source, and the angle between incident and scattered

[c]Scattering off fast-moving coronal electrons does, however, broaden and decrease the contrast of photospheric spectral features.

rays is not exactly 90°, accurate calculation of polarization is more complicated.[8,27] However, the scattered radiation is still highly polarized, and the 90° ("plane of the sky") approximation is adequate out to $\sim 70\ R_\odot$.[27]

For a ground-based K-coronagraph, the main source of background linear polarization is sunlight scattered from the atmosphere, either directly or after reflection from the Earth; Ref. 28 discusses the accuracy to which this background can removed by calibration. For a space-based K-coronagraph, the only significant source of background linear polarization is the F-corona. Both the radiance and the polarization of the zodiacal light are functions of ecliptic latitude and longitude and are relatively poorly known for solar elongation angles less than about 10°.[22] Reference 29 infers that the polarization is negligible inside 5 $R_\odot$ and reaches 0.8% at 16 $R_\odot$ but cautions that better measurements are strongly needed. Nonetheless, the K-corona is more highly polarized, so polarization-sensitive measurements increase the signal-to-noise ratio of a coronagraph. The offsetting penalty is an increase in the complexity and duration of the measurement.

### 3.2.2. *Polarimetry*

Incoherent, partially polarized light may be characterized in a time average by four so-called Stokes parameters, $\{I, Q, U, V\}$, representing, respectively, the total intensity (radiance or irradiance) within some bandpass, the intensities of two independent states of linear polarization, and the intensity of circular polarization.[30] At least three measurements must be taken to determine $I$, $Q$, and $U$; $V$ is generally not measured unless the instrument determines the strength of the magnetic field in the low corona using the Zeeman effect. In space-based coronagraphs, two common arrangements are three successive measurements through polarizers with axes at 0°, 60°, and 120°, or three measurements through polarizers with axes at 0°, 45°, and 90° (a fourth measurement at 135° may be included for redundancy). In a ground-based coronagraph, the polarized noise induced by atmospheric seeing can be overcome by using fast electro-optical variable retarders and a polarizing beamsplitter (analyzer) to produce a rapidly modulated irradiance signal at the detector(s) that can be used to recover the Stokes parameters.[31,32]

All optical systems introduce instrumental polarization that must be calibrated and removed. The goal is to derive a so-called instrument Mueller matrix, $M$, that connects the Stokes vector of light entering the instrument, $S_{\rm in}$, with the Stokes vector of light at the focal plane, $S_{\rm out}$, through the linear transformation $S_{\rm out} = MS_{\rm in}$.[30] References 28 and 33 describe representative calibration procedures for, respectively, a ground-based and two space-based polarimetric coronagraphs.

## 4. Design Principles

The French astronomer Bernard Lyot invented the coronagraph in the 1930s and used it to obtain coronal images without a solar eclipse for the first time.[34] His most notable innovation was the introduction of an aperture (the Lyot stop) to block light diffracted around the entrance aperture, but the success of his instruments required unusual care in many respects, including a high-altitude observing site, immaculately clear and dust-free lenses, and systematic blocking of stray light. Lyot's approach holds an enduring lesson for contemporary coronagraph designers: despite decades of instrument heritage and powerful computational tools, it is still easy to build a coronagraph that does not work.

### 4.1. *The Basic Coronagraph*

As a coronagraph is sometimes described as creating an artificial eclipse, one's first thought might be to emulate the moon—to "put a thumb over the Sun." This fails because an external occulter by itself does not adequately control diffracted light unless it is quite distant from the entrance aperture (Section 4.2). Lyot's great insight was to realize that light diffracting around a system aperture could be suppressed by re-imaging it and blocking its bright rim with another aperture. The same principle applies to occulters. Figure 6 serves to illustrate a circularly symmetric coronagraph design with both external and internal occulting. Lyot's coronagraphs used only internal occulting. Evans[35] added an external occulter to the basic Lyot design.

From left to right in Fig. 6, a front aperture blocks stray light from outside the desired field of view. The external occulter (D1, shown as three closely-spaced obstacles) ensures that the full entrance aperture (A1) is shaded from photospheric light. At the image plane of the objective lens (O1), a field stop aperture defines the field of view. If there is no external occulter, it is also necessary to place an occulter (or Lyot mask) at or near the image plane of the objective lens to keep light and heat from the image of the solar disk from reaching further into the system; however, this occulter does not suppress diffraction.[37] Next is an internal occulter (D2) at an image of the external occulter, slightly larger than that image in order to block its bright rim of diffracted light. A second lens reimages the entrance aperture onto the Lyot stop (A3), an aperture slightly smaller than the image, again blocking its bright rim. A final lens (O3) creates the image of the occulted Sun on the final focal plane (F). A small reflecting spot is often placed in the center of this lens in order to block an out-of-focus solar image created by multiple reflections in the objective lens.[34,38]

Many variations are possible on the basic design illustrated in Fig. 6. An objective lens is usually a high-purity singlet or doublet in order to minimize small-angle scattering, but following lenses may be more complicated. A filter or polarizer may be placed in locations other than the one shown. One or more of the lenses may be replaced by a mirror; if the objective is a mirror, the instrument is called a reflecting coronagraph.

The external/internal occulter pair and the Lyot stop each has the potential to reduce stray light by about six orders of magnitude, with the result that the

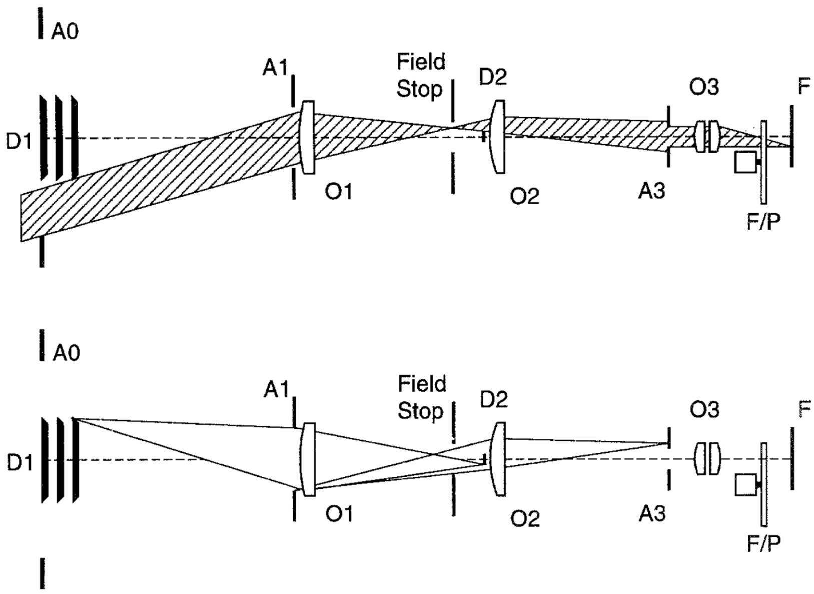


Fig. 6. Schematic layout of the LASCO C3 coronagraph on the SOHO satellite.[36] The top diagram illustrates image formation; the bottom diagram shows how stray light is blocked from reaching the image plane. Sunlight enters from the left. Components shown: front aperture A0, external occulter D1, entrance aperture A1, objective lens O1, internal occulter D2, field lens O2, Lyot stop A3, relay lens with Lyot spot O3, filter/polarizer wheels and shutter F/P, and focal plane F.

most sensitive solar coronagraphs suppress stray light to the order of $10^{-12}$ of the radiance of the solar disk.[39] There is currently strong interest in a coronagraph that can be accommodated on a small satellite, particularly for the purpose of monitoring space weather. It has been shown theoretically and experimentally that, by careful placement of the internal occulter and field lens, diffractive light can be suppressed by about 9 orders of magnitude even when the Lyot stage is eliminated; however, this level of suppression is achieved only over a limited radius range, $3 \lesssim R_\odot \lesssim 12$.[40,41]

### 4.2. *External Occulters*

An external occulter (EO) influences the performance of a coronagraph in three main ways.

(1) The EO must shade the entire entrance aperture (EA) from direct sunlight. This requires that the radius of the occulting disk satisfy $r_{\rm oc} \geq a + d \tan\theta_\odot$, where $a$ is the radius of the EA, $d$ is the separation between the EO and the EA, and $\theta_\odot$ is the angular radius of the Sun.
(2) The EO partially shades (vignettes) the EA from coronal light for angular radii that satisfy $r_{\rm oc} - a < d \tan\theta < r_{\rm oc} + a$. Vignetting reduces the coronal flux

reaching the EA and reduces the angular resolution of the system.
(3) Light diffracts around and scatters from the EO.

### 4.2.1. *Vignetting*

The designer must choose $r_{oc}$, $d$, and $a$ to be consistent with scientific requirements, including angular resolution, temporal resolution, and the range of solar radii to be observed, as well as practical limitations on the size of the system imposed by manufacturability and cost. Suppose that $a$ has been chosen. Simple geometry[42] yields the vignetted fraction as a function of $d/a$ and the inner (smallest unocculted) field angle, $\theta_{\text{min}}$; this fraction is approximately linear, decreasing from 1 at $\theta_{\text{min}} \approx (r_{oc} - a)/d$ to 0 at $\theta_{\text{free}} \approx (r_{oc} + a)/d$. Vignetting is a design tool as well as a constraint because it partially counteracts the steep radiance gradient of the corona (Fig. 3.1) and thereby reduces the dynamic range of the signal that must be accommodated by the focal plane array. Reference 42 shows that the angular resolution afforded by the vignetted EA, normalized to the resolution of the full EA, is well approximated by $(1 - v)^{-1/2}$, where $v$ is the vignetted fraction. Figure 7 illustrates the effects of vignetting on normalized flux and angular resolution. Achieving good angular resolution close to the solar limb requires a relatively distant external occulter. Such an occulter may be located at the end of a boom or, in space, on a separate spacecraft from the craft carrying the rest of the optics and the detector system.[43]

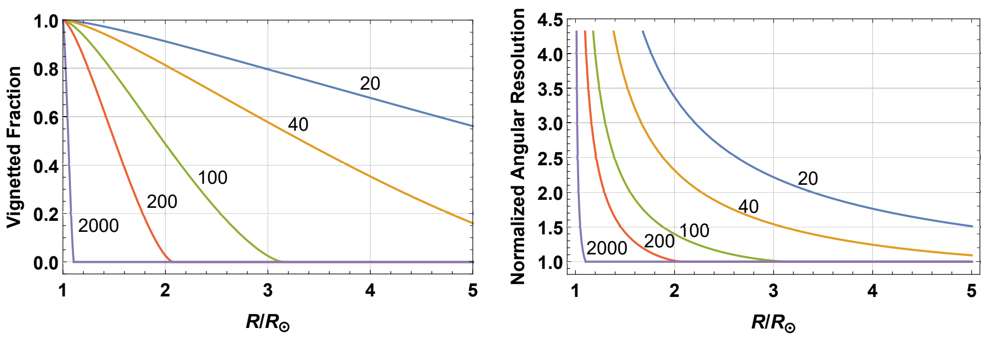


Fig. 7. Left: Fraction of the area of the entrance aperture vignetted by the external occulter for various values of $d/a$, where $a$ is the radius of the entrance aperture and $d$ is the separation between the external occulter and the entrance aperture. Right: The effect of vignetting on resolution, normalized to the resolution of the unobscured entrance aperture, for the same values of $d/a$.

### 4.2.2. *Diffraction*

Diffraction around the EO is unavoidable, hence the need for an internal occulter (IO) to accomplish for the EO what the Lyot stop does for the EA. Because diffracted light that reaches the EA influences all later optical stages, it is important to know how the diffractive illumination of the EA varies with distance to the EO and the amount that it over-occults. Fresnel diffraction theory is applicable because the EA is in the near field of the EO. Although few Fresnel diffraction problems can be solved analytically,[44] simple cases provide useful guidance. Consider a square EO normally illuminated by a point source. The complex field distribution at the EA can be expressed in terms of Fresnel integrals,[45] and, at the center of the EA, is a function only of the Fresnel number of the EO as seen from the EA, $\mathcal{F} = r_{\rm oc}^2/\lambda d$. For practical solar coronagraphs, $\mathcal{F} \gtrsim 100$, which leads to the simple approximation that the irradiance at the center of the EA is $4/(\pi^2\mathcal{F})$. With the substitution $r_{\rm oc} = f_{\rm oc}(a + d\tan\theta_\odot)$, where $f_{\rm oc} \geq 1$ is the over-occulting factor, the maximum of central irradiance occurs at an occulter distance of $a/(f_{\rm oc}\tan\theta_\odot)$ with value $\lambda/(f_{\rm oc}\pi^2 a\tan\theta_\odot)$. Note that the maximum irradiance is proportional to $a^{-1}$ and the EO distance at which this occurs is proportional to $a$. Figure 8 compares the behavior of the simple relationship $4/(\pi^2\mathcal{F})$ with accurate calculations that integrate over the solar disk for two values of the EA radius.[d] The simple relationship captures the maximum irradiance but not the shape of the curves. Significantly, the effectiveness of the external occulter does not vary dramatically over the range of occulter distances applicable to a single spacecraft (0.5–20 m): less than a factor of 10 for a 5-mm (radius) entrance aperture and less than a factor of 2 for a 50-mm entrance aperture.

In practical implementation, the effectiveness of the EO can be increased significantly by using more than a simple opaque disk as the occulter. Examples include a serrated single disk;[46] two or more disks arranged along the optical axis so that each disk both shadows the next disk from direct sunlight and blocks some of the light that diffracts around the previous disk;[38,40] a threaded barrel or truncated cone that approximates a many-disk system with a continuous structure;[38,47] or an unthreaded (rough or smooth) structure that could potentially have a free-form shape. Until recently, the design of external occulters was guided mainly by experience and experiment. Reference 48 discusses the history, theoretical analysis, and performance testing of compound external occulters and includes examples of numerically optimized configurations.

### 4.3. *End-to-End Diffractive Analysis*

The schematic description of a coronagraph in Sec. 4.1 does not quantify at least two important aspects of diffractive performance (in addition to the characteristics of the external occulter, discussed above): the radius of the internal occulter ($\geq 1$ in units of the radius of the external occulter image) and the radius of the Lyot stop ($\leq 1$ in units of the entrance pupil image). End-to-end diffractive analysis can be accomplished using Fourier optics.[37,45] Figure 9 illustrates the combined effects of the EO and the Lyot stop on residual diffracted sunlight for the ASPIICS orbiting

[d] In solar diffraction computations, integrating over the solar disk is more laborious than a point-source calculation but necessary for accurate results.

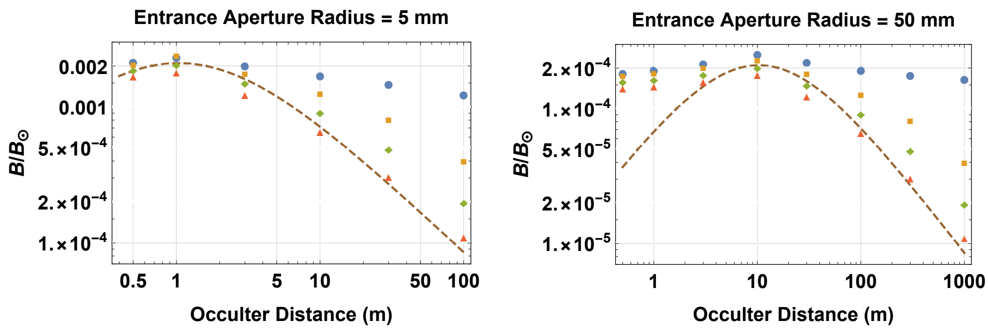


Fig. 8. Irradiance integrated over an entrance aperture of radius 5-mm (left) or 50-mm (right),in units of the unocculted value, as a function of external occulter distance. Dashed curve: $4/(\pi^2\mathcal{F})$. Dots (top to bottom): over-occulting factor 1.0, 1.03, 1.05, 1.1. Wavelength: 500 nm.

coronagraph currently in development.[18,49]

## 5. Some Practical Considerations

### 5.1. *Non-diffractive Stray Light*

As indicated in Sec. 2, it is difficult to generalize about controlling non-diffractive stray light because of the range of potential sources external and internal to the coronagraph. The primary external source is always the solar disk. In space, secondary external sources may include earthshine or spacecraft structures such as

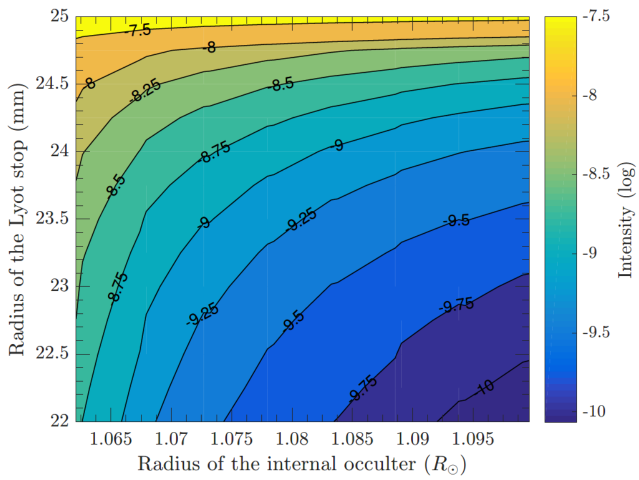


Fig. 9. Contour map of residual diffracted sunlight expected at 1.3 $R_\odot$ for the proposed ASPIICS space coronagraph.[18] The vertical scale spans 0.88–1.0 in units of the radius of the entrance pupil image; the horizontal scale spans 1.005–1.04 in units of the radius of the external occulter image. The intensity scale is normalized to the mean intensity of the solar disk.

solar panels. On the ground, the sky (solar light scattered by gases and particulates in the atmosphere) is always a limiting external source, even at the best observing sites. Internal sources within the instrument field of view include scattering from inclusions and bubbles within lenses and scattering from particulates and microscopic irregularities on optical surfaces. Other internal sources include diffuse or specular reflection from structural components of the instrument. Scattering from dust and optical imperfections is particularly troublesome because it cannot be eliminated from the optical path to focus, hence the need for scrupulous contamination control throughout the fabrication and testing of coronagraphs. Figure 10 illustrates the significant effect a single dust particle can have on the stray light performance of a coronagraph.

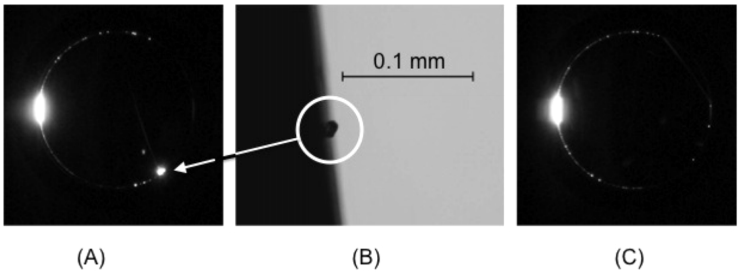


Fig. 10. The effect of a single 12 $\mu$m dust particle on stray light in the METIS coronagraph for the Solar Orbiter mission.[50] (A) The contaminated external occulter as seen off-axis from the position of the objective mirror of the coronagraph. (B) Micrograph of the edge of the occulter showing the offending particle with an arrow indicating its effect in (A). (C) Same as (A) with a clean occulter.

Coronagraphs always include annular baffles along the optical path (Fig. 11). If there is no external occulter, the internal occulter may be cone-shaped to send direct light from the solar disk into a surrounding light trap.[51] In an externally occulted system, there is typically a heat rejection mirror,[36,51] which is a potential source of stray light.

The quantitative analysis of stray light is carried out with specialized software that allows for both sequential (geometrical optics) and non-sequential propagation. There are a number of commercial programs (*e.g.*, ASAP®, FRED™, LightTools®, OpticStudio®, TracePro®) as well as at least one open-source program.[52] The user defines sources and detectors of radiation within an optomechanical environment that includes both imaging and non-imaging components. The software launches a large number of rays and follows them as they refract, reflect, scatter, and terminate according to user-specified properties. As a coronagraph requires very low stray light levels in the focal plane, a full analysis typically requires a substantial effort; the process of inserting and modifying baffles, traps and coatings is iterative even for an experienced analyst. The scattering properties of a surface are characterized by a bidirectional scatter distribution function (BSDF).[53] Discussion of BSDFs relevant

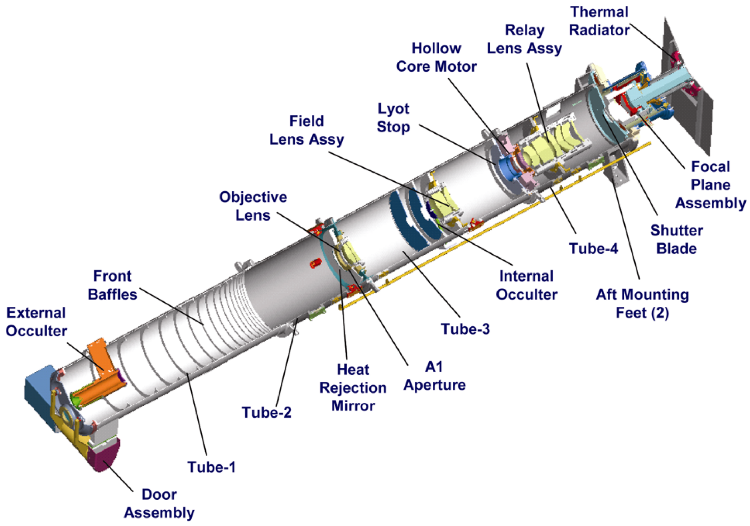


Fig. 11. Cutaway illustration of the optomechanical layout of the COR2 externally occulted space coronagraph.[51]

to coronagraphs may be found in Refs. 54, 55, and 56.

### 5.2. *Signal-to-Noise Ratio*

The signal from the solar K-corona was discussed in Sec. 3.1. The main equations necessary to estimate signal-to-noise ratio (SNR) are the camera equation[57] and the so-called CCD equation,[58] also applicable to CMOS sensors. The camera equation relates the radiance $R$ (photon $\mathrm{s}^{-1}\,\mathrm{m}^{-2}\,\mathrm{sr}^{-1}$) of the source to the irradiance $I$ (photon $\mathrm{s}^{-1}\,\mathrm{m}^{-2}$) in the focal plane:

$$I = \pi t R[(2f\#_{\mathrm{min}})^{-2} - (2f\#_{\mathrm{max}})^{-2}]$$

where $t$ is the throughput of the optical system (including the quantum efficiency of the detector) and $f\#_{\mathrm{min}}$ and $f\#_{\mathrm{max}}$ denote the minimum and maximum angular subtense, expressed as an $f$-number, of a system that may have a central obstruction such as an external occulter. The CCD equation gives the SNR as

$$\mathrm{SNR} = \frac{\mathrm{N_{signal}}}{\sqrt{\mathrm{N_{signal}} + \mathrm{n_{pix}}(1 + (\mathrm{n_{pix}}/\mathrm{n_{bg}}))(\mathrm{N_{bg}} + \mathrm{N_D} + \mathrm{N_R^2} + \mathrm{G^2}\sigma_\mathrm{f}^2)}}$$

where $N_{\mathrm{signal}}$ is the total number of signal photons detected during a single exposure from a region comprising $n_{\mathrm{pix}}$ pixels, $n_{\mathrm{bg}}$ is the number of pixels used to determine the background (*e.g.*, the F-corona, or the atmosphere for a ground-based coronagraph), $N_{\mathrm{bg}}$ is the photon count from the background, $N_D$ is the detector dark current in electrons, $N_R$ is the detector read noise in electrons, $G$ is the detector gain in electrons per data number, and $\sigma_f$ accounts for digitization noise (typically $\sigma_f \simeq 0.29$). Because of structure and time-variability in the background, the SNR derived from this equation must be treated as a design tool rather than a firm predictor of system performance.

### 5.3. *Performance Testing*

The performance testing of solar coronagraph components can often be accomplished in a conventional laboratory of sufficient and consistent cleanliness; the degraded stray-light performance illustrated in Fig. 10 was the intentional result of only 3 days of exposure in a ISO7/8 (Class 10,000/100,000) environment after 3 months in an ISO5 (Class 100) cleanroom.[50] For spaceborne far or extreme ultraviolet coronagraphs, attention must also be paid to molecular contaminants that can polymerize when exposed on orbit to solar UV radiation and severely degrade the FUV/EUV sensitivity of the instrument.[59]

End-to-end testing of the full system requires a specialized facility.[60–63] A simulated solar source must be provided, of the correct angular extent and bright enough that stray light as weak as $10^{-8}$–$10^{-12}$ of the source radiance can be recorded by the detector. Stray light levels, photometric calibration, and image quality are best done in vacuum to eliminate scattering by airborne dust and degradation of the image by atmospheric turbulence. End-to-end testing poses a particular challenge for space-based formation-flying coronagraphs, such as the ASPIICS instrument under development for the ESA PROBA-3 mission, in which the occulter spacecraft is 150 m in front of the detector spacecraft.[49] References 64–65 discuss the theoretical basis for and practical realization of scaled model instruments that can be tested in existing facilities and yet quantitatively capture the diffractive behavior of the full-scale system. The absolute radiometric calibration of a coronagraph can be established on the ground and tracked on orbit using celestial sources such as planets and stars.[66]

## Acknowledgments

I am grateful to F. Landini and O. C. St. Cyr for their comments on the manuscript. This work was funded by the National Aeronautics and Space Administration.

## References

1. J. Toomre and M. J. Thompson, Prospects and Challenges for Helioseismology, *Space Science Reviews*. **196**(1-4), 1–14 (Dec, 2015). doi: 10.1007/s11214-015-0147-x.
2. C. E. Parnell and I. De Moortel, A contemporary view of coronal heating, *Philosophical Transactions of the Royal Society of London Series A*. **370**(1970), 3217–3240 (Jul, 2012). doi: 10.1098/rsta.2012.0113.
3. M. J. Aschwanden, A. I. Poland, and D. M. Rabin, The New Solar Corona, *Annual Review of Astronomy and Astrophysics*. **39**, 175–210 (Jan, 2001). doi: 10.1146/annurev.astro.39.1.175.
4. P. V. Foukal, *Solar Astrophysics, 2nd, Revised Edition*. 2004.

5. P. J. Cargill, Coronal Magnetism: Difficulties and Prospects, *Space Science Reviews.* **144**(1-4), 413–421 (Apr, 2009). doi: 10.1007/s11214-008-9446-9.
6. N. E. Raouafi, P. Riley, S. Gibson, S. Fineschi, and S. K. Solanki, Diagnostics of Coronal Magnetic Fields Through the Hanle Effect in UV and IR Lines, *Frontiers in Astronomy and Space Sciences.* 3:20 (Jun, 2016). doi: 10.3389/fspas.2016.00020.
7. S. R. Habbal, M. Druckmüller, H. Morgan, A. Ding, J. Johnson, H. Druckmüllerová, A. Daw, M. B. Arndt, M. Dietzel, and J. Saken, Thermodynamics of the Solar Corona and Evolution of the Solar Magnetic Field as Inferred from the Total Solar Eclipse Observations of 2010 July 11, *Astrophysical Journal.* 734(2):120 (Jun, 2011). doi: 10.1088/0004-637X/734/2/120.
8. D. E. Billings, *A guide to the solar corona.* 1966.
9. D. B. Seaton, A. De Groof, P. Shearer, D. Berghmans, and B. Nicula, SWAP Observations of the Long-term, Large-scale Evolution of the Extreme-ultraviolet Solar Corona, *Astrophysical Journal.* 777(1):72 (Nov, 2013). doi: 10.1088/0004-637X/777/1/72.
10. Spectacular erupting filament with earth-directed space weather (Sept., 2013). URL `http://www.thesuntoday.org/space-weather/spectacular-erupting-filament-with-earth-directed-space-weather/`.
11. V. H. Hansteen and M. Velli, Solar Wind Models from the Chromosphere to 1 AU, *Space Science Reviews.* **172**(1-4), 89–121 (Nov, 2012). doi: 10.1007/s11214-012-9887-z.
12. L. Fletcher, B. R. Dennis, H. S. Hudson, S. Krucker, K. Phillips, A. Veronig, M. Battaglia, L. Bone, A. Caspi, and Q. Chen, An Observational Overview of Solar Flares, *Space Science Reviews.* **159**(1-4), 19–106 (Sep, 2011). doi: 10.1007/s11214-010-9701-8.
13. D. F. Webb and T. A. Howard, Coronal Mass Ejections: Observations, *Living Reviews in Solar Physics.* 9(1):3 (Jun, 2012). doi: 10.12942/lrsp-2012-3.
14. M. Yamada, R. Kulsrud, and H. Ji, Magnetic reconnection, *Reviews of Modern Physics.* **82**(1), 603–664 (Jan, 2010). doi: 10.1103/RevModPhys.82.603.
15. A. K. Singh, D. Siingh, and R. P. Singh, Space Weather: Physics, Effects and Predictability, *Surveys in Geophysics.* **31**(6), 581–638 (Dec, 2010). doi: 10.1007/s10712-010-9103-1.
16. R. A. Howard, A. Vourlidas, C. M. Korendyke, S. P. Plunkett, M. T. Carter, D. Wang, N. Rich, D. R. McMullin, S. Lynch, and A. Thurn. The solar and heliospheric imager (SoloHI) instrument for the solar orbiter mission. In *Solar Physics and Space Weather Instrumentation V*, vol. 8862, *Society of Photo-Optical Instrumentation Engineers (SPIE) Conference Series*, p. 88620H (Sep, 2013). doi: 10.1117/12.2027657.
17. E. Fest, *Stray light analysis and control.* (SPIE Press, 2013). doi: 10.1117/3.1000980.
18. R. Rougeot, R. Flamary, D. Galano, and C. Aime, Performance of the hybrid externally occulted Lyot solar coronagraph. Application to ASPIICS, *Astronomy and Astrophysics.* 599:A2 (Mar, 2017). doi: 10.1051/0004-6361/201629259.
19. C. Lebecq, S. Koutchmy, and G. Stellmacher, The 1981 total solar eclipse corona. II. Global absolute photometric analysis., *Astronomy and Astrophysics.* **152**, 157–164 (Nov, 1985).
20. H. Lin and M. J. Penn, The Advanced Technology Solar Telescope Site Survey Sky Brightness Monitor, *Publications of the Astronomical Society of the Pacific.* **116**(821), 652–666 (Jul, 2004). doi: 10.1086/422205.
21. L. Golub and J. M. Pasachoff, *The Solar Corona.* 2009.
22. C. Leinert, S. Bowyer, L. K. Haikala, M. S. Hanner, M. G. Hauser, A. C. Levasseur-Regourd, I. Mann, K. Mattila, W. T. Reach, and W. Schlosser, The 1997 reference of diffuse night sky brightness, *Astronomy and Astrophysics, Supplement.* **127**, 1–99

(Jan, 1998). doi: 10.1051/aas:1998105.
23. S. Koutchmy and P. L. Lamy. The F-Corona and the Circum-Solar Dust Evidences and Properties (ir). In eds. R. H. Giese and P. Lamy, *IAU Colloq. 85: Properties and Interactions of Interplanetary Dust*, p. 63 (Jan, 1985). doi: 10.1007/978-94-009-5464-9_14.
24. H. Lin, J. R. Kuhn, and R. Coulter, Coronal Magnetic Field Measurements, *Astrophysical Journal*. **613**(2), L177–L180 (Oct, 2004). doi: 10.1086/425217.
25. M. J. Penn, H. Lin, S. Tomczyk, D. Elmore, and P. Judge, Background-Induced Measurement Errors of the Coronal Intensity, Density, Velocity, and Magnetic Field, *Solar Physics*. **222**(1), 61–78 (Jul, 2004). doi: 10.1023/B:SOLA.0000036850.34404.5f.
26. A. G. de Wijn, S. Tomczyk, and J. Burkepile. A Progress Update for the COronal Solar Magnetism Observatory for Coronal and Chromospheric Polarimetry. In eds. K. N. Nagendra, J. O. Stenflo, Q. Qu, and M. Samooprna, *Solar Polarization 7*, vol. 489, *Astronomical Society of the Pacific Conference Series*, p. 323 (Oct, 2014).
27. A. Vourlidas and R. A. Howard, The Proper Treatment of Coronal Mass Ejection Brightness: A New Methodology and Implications for Observations, *Astrophysical Journal*. **642**(2), 1216–1221 (May, 2006). doi: 10.1086/501122.
28. D. F. Elmore, J. T. Burkepile, J. A. Darnell, A. R. Lecinski, and A. L. Stanger. Calibration of a ground-based solar coronal polarimeter. In ed. S. Fineschi, *Polarimetry in Astronomy*, vol. 4843, *Society of Photo-Optical Instrumentation Engineers (SPIE) Conference Series*, pp. 66–75 (Feb, 2003). doi: 10.1117/12.459279.
29. I. Mann, The solar F-corona: calculations of the optical and infrared brightness of circumstellar dust., *Astronomy and Astrophysics*. **261**, 329–335 (Jul, 1992).
30. J. Tinbergen, *Astronomical Polarimetry*. 1996.
31. S. Tomczyk, R. Casini, A. G. de Wijn, and P. G. Nelson, Wavelength-diverse polarization modulators for Stokes polarimetry, *Applied Optics*. **49**(18), 3580 (Jun, 2010). doi: 10.1364/AO.49.003580.
32. J. Hou, A. G. de Wijn, and S. Tomczyk, Design and measurement of the Stokes polarimeter for the COSMO K-coronagraph, *Astrophysical Journal*. 774(1):85 (Sep, 2013). doi: 10.1088/0004-637X/774/1/85.
33. T. G. Moran, J. M. Davila, J. S. Morrill, D. Wang, and R. Howard, Solar and Heliospheric Observatory/Large Angle Spectrometric Coronagraph Polarimetric Calibration, *Solar Physics*. **237**(1), 211–222 (Aug, 2006). doi: 10.1007/s11207-006-0147-9.
34. B. Lyot, The study of the solar corona and prominences without eclipses (George Darwin Lecture, 1939), *Monthly Notices of the Royal Astronomical Society*. **99**, 580 (Jun, 1939). doi: 10.1093/mnras/99.8.580.
35. J. W. Evans, Photometer for measurement of sky brightness near the sun, *Journal of the Optical Society of America (1917-1983)*. **38**(12), 1083 (Dec, 1948).
36. G. E. Brueckner, R. A. Howard, M. J. Koomen, C. M. Korendyke, D. J. Michels, J. D. Moses, D. G. Socker, K. P. Dere, P. L. Lamy, and A. Llebaria, The Large Angle Spectroscopic Coronagraph (LASCO), *Solar Physics*. **162**(1-2), 357–402 (Dec, 1995). doi: 10.1007/BF00733434.
37. F. Malbet, High angular resolution coronography for adaptive optics., *Astronomy and Astrophysics, Supplement*. **115**, 161 (Jan, 1996).
38. J. Newkirk, Gordon and D. Bohlin, Reduction of scattered light in the coronagraph, *Applied Optics*. **2**, 131 (Feb, 1963). doi: 10.1364/AO.2.000131.
39. R. A. Howard, Recent white-light coronagraphs at the Naval Research Laboratory, *Applied Optics*. **54**(31), F298 (Nov, 2015). doi: 10.1364/AO.54.00F298.
40. Q. Gong and D. Socker. Theoretical study of the occulted solar coronagraph. In eds. P. T. C. Chen, J. C. Fleming, and M. G. Dittman, *Optical Systems Degradation, Contamination, and Stray Light: Effects, Measurements, and Control*, vol. 5526, *Society*

*of Photo-Optical Instrumentation Engineers (SPIE) Conference Series*, pp. 208–219 (Oct, 2004). doi: 10.1117/12.549275.
41. N. Gopalswamy and Q. Gong. A small satellite mission for solar coronagraphy. In *Society of Photo-Optical Instrumentation Engineers (SPIE) Conference Series*, vol. 10769, *Society of Photo-Optical Instrumentation Engineers (SPIE) Conference Series*, p. 107690X (Sep, 2018). doi: 10.1117/12.2323807.
42. A. R. Bayanna, S. K. Mathew, K. Sankarasubramanian, P. Venkatakrishnan, J. Singh, and B. R. Prasad, Issues with external occultation of a coronagraph, *Experimental Astronomy*. **29**(3), 145–153 (Apr, 2011). doi: 10.1007/s10686-010-9207-0.
43. P. Lamy and S. Vivès, New perspective in solar coronal physics: Giant externally occulted coronagraphs using satellites in flight formation, *Acta Astronautica*. **65**, 273–278 (Jul, 2009). doi: 10.1016/j.actaastro.2009.01.060.
44. M. Born and E. Wolf, *Principles of Optics*. 1999.
45. J. W. Goodman, *Introduction to Fourier optics*. 2005.
46. J. D. Purcell and M. J. Koomen, Coronagraph with improved scattered light properties, *Report of NRL Progress*. **9**, 9–14, (1962).
47. S. Koutchmy and M. Belmahdi, Improved measurements of scattered light level behind occulting systems., *Journal of Optics*. **18**(5), 265–269 (Jan, 1987). doi: 10.1088/0150-536X/18/5-6/008.
48. F. Landini, S. Vives, M. Venet, M. Romoli, C. Guillon, and S. Fineschi, External occulter laboratory demonstrator for the forthcoming formation flying coronagraphs, *Applied Optics*. **50**(36), 6632 (Dec, 2011). doi: 10.1364/AO.50.006632.
49. E. Renotte, A. Alia, A. Bemporad, J. Bernier, C. Bramanti, S. Buckley, G. Capobianco, I. Cernica, V. Dániel, and R. Darakchiev. Design status of ASPIICS, an externally occulted coronagraph for PROBA-3. In *Solar Physics and Space Weather Instrumentation VI*, vol. 9604, *Society of Photo-Optical Instrumentation Engineers (SPIE) Conference Series*, p. 96040A (Sep, 2015). doi: 10.1117/12.2186962.
50. F. Landini, M. Romoli, G. Capobianco, S. Vives, S. Fineschi, G. Massone, D. Loreggia, E. Turchi, C. Guillon, and C. Escolle. Improved stray light suppression performance for the solar orbiter/METIS inverted external occulter. In *Solar Physics and Space Weather Instrumentation V*, vol. 8862, *Society of Photo-Optical Instrumentation Engineers (SPIE) Conference Series*, p. 886204 (Sep, 2013). doi: 10.1117/12.2024209.
51. R. A. Howard, J. D. Moses, A. Vourlidas, J. S. Newmark, D. G. Socker, S. P. Plunkett, C. M. Korendyke, J. W. Cook, A. Hurley, and J. M. Davila, Sun Earth Connection Coronal and Heliospheric Investigation (SECCHI), *S*. **136**(1-4), 67–115 (Apr, 2008). doi: 10.1007/s11214-008-9341-4.
52. F. Mauch, M. Gronle, W. Lyda, and W. Osten, Open-source graphics processing unit-accelerated ray tracer for optical simulation, *Optical Engineering*. 52:053004 (May, 2013). doi: 10.1117/1.OE.52.5.053004.
53. J. C. Stover, *Optical scattering. Measurement and analysis*. 1995.
54. F. Landini, M. Romoli, S. Vives, C. Baccani, C. Escolle, M. Pancrazzi, M. Focardi, V. Da Deppo, J. D. Moses, and S. Fineschi. Coating and surface finishing definition for the Solar Orbiter/METIS inverted external occulter. In *Advances in Optical and Mechanical Technologies for Telescopes and Instrumentation*, vol. 9151, *Society of Photo-Optical Instrumentation Engineers (SPIE) Conference Series*, p. 91515H (Jul, 2014). doi: 10.1117/12.2056331.
55. G. L. Peterson. A BRDF model for scratches and digs. In *Reflection, Scattering, and Diffraction from Surfaces III*, vol. 8495, *Society of Photo-Optical Instrumentation Engineers (SPIE) Conference Series*, p. 84950G (Oct, 2012). doi: 10.1117/12.930860.
56. P. Sandri, S. Fineschi, M. Romoli, M. Taccola, F. Landini, V. Da Deppo, G. Naletto,

D. Morea, D. Naughton, and E. Antonucci, Stray-light analyses of the multielement telescope for imaging and spectroscopy coronagraph on Solar Orbiter, *Optical Engineering*. 57:015108 (Jan, 2018). doi: 10.1117/1.OE.57.1.015108.

57. G. Paez-Padilla and M. S. Scholl. Camera equation for an optical system with an on-axis obscuration. In eds. M. S. Scholl and B. F. Andresen, *Infrared Spaceborne Remote Sensing IV*, vol. 2817, *Society of Photo-Optical Instrumentation Engineers (SPIE) Conference Series*, pp. 231–236 (Oct, 1996). doi: 10.1117/12.255192.
58. W. J. Merline and S. B. Howell, A Realistic Model for Point-sources Imaged on Array Detectors: The Model and Initial Results, *Experimental Astronomy*. **6**(1-2), 163–210 (Jan, 1995). doi: 10.1007/BF00421131.
59. A. BenMoussa, S. Gissot, U. Schühle, G. Del Zanna, F. Auchère, S. Mekaoui, A. R. Jones, D. Walton, C. J. Eyles, and G. Thuillier, On-Orbit Degradation of Solar Instruments, *Solar Physics*. **288**(1), 389–434 (Nov, 2013). doi: 10.1007/s11207-013-0290-z.
60. J. S. Morrill, C. M. Korendyke, G. E. Brueckner, F. Giovane, R. A. Howard, M. Koomen, D. Moses, S. P. Plunkett, A. Vourlidas, and E. Esfandiari, Calibration of the Soho/Lasco C3 White Light Coronagraph, *Solar Physics*. **233**(2), 331–372 (Feb, 2006). doi: 10.1007/s11207-006-2058-1.
61. W. T. Thompson, J. M. Davila, R. R. Fisher, L. E. Orwig, J. E. Mentzell, S. E. Hetherington, R. J. Derro, R. E. Federline, D. C. Clark, and P. T. C. Chen. COR1 inner coronagraph for STEREO-SECCHI. In eds. S. L. Keil and S. V. Avakyan, *Innovative Telescopes and Instrumentation for Solar Astrophysics*, vol. 4853, *Society of Photo-Optical Instrumentation Engineers (SPIE) Conference Series*, pp. 1–11 (Feb, 2003). doi: 10.1117/12.460267.
62. S. Fineschi, G. Crescenzio, G. Massone, G. Capobianco, L. Zangrilli, E. Antonucci, and F. Anselmi. OPSys: optical payload systems facility for testing space coronagraphs. In *Solar Physics and Space Weather Instrumentation IV*, vol. 8148, *Society of Photo-Optical Instrumentation Engineers (SPIE) Conference Series*, p. 81480W (Oct, 2011). doi: 10.1117/12.897794.
63. M. E., Y. , Stockman, and M. L. M. Hellin. Design and modelisation of a straylight facility for space optical instrument. In *Optical Systems Design 2012*, vol. 8550, *Society of Photo-Optical Instrumentation Engineers (SPIE) Conference Series*, (2012). doi: 10.1117/12.981159. URL `https://doi.org/10.1117/12.981159`.
64. F. Landini, M. Romoli, C. Baccani, M. Focardi, M. Pancrazzi, D. Galano, and V. Kirschner, Scaled-model guidelines for formation-flying solar coronagraph missions, *Optics Letters*. **41**(4), 757 (Feb, 2016). doi: 10.1364/OL.41.000757.
65. F. Landini, C. Baccani, S. Vives, S. Fineschi, M. Romoli, G. Capobianco, G. Massone, M. Casti, A. Bemporad, and M. Focardi. Test plan for the PROBA3/ASPIICS scaled model measurement campaign. In *Society of Photo-Optical Instrumentation Engineers (SPIE) Conference Series*, vol. 10397, *Society of Photo-Optical Instrumentation Engineers (SPIE) Conference Series*, p. 103971C (Aug, 2017). doi: 10.1117/12.2273921.
66. W. T. Thompson, J. M. Davila, O. C. St. Cyr, and N. L. Reginald, STEREO SECCHI COR1-A/B Intercalibration at 180 degree Separation, *Solar Physics*. **272**(1), 215–225 (Aug, 2011). doi: 10.1007/s11207-011-9815-5.